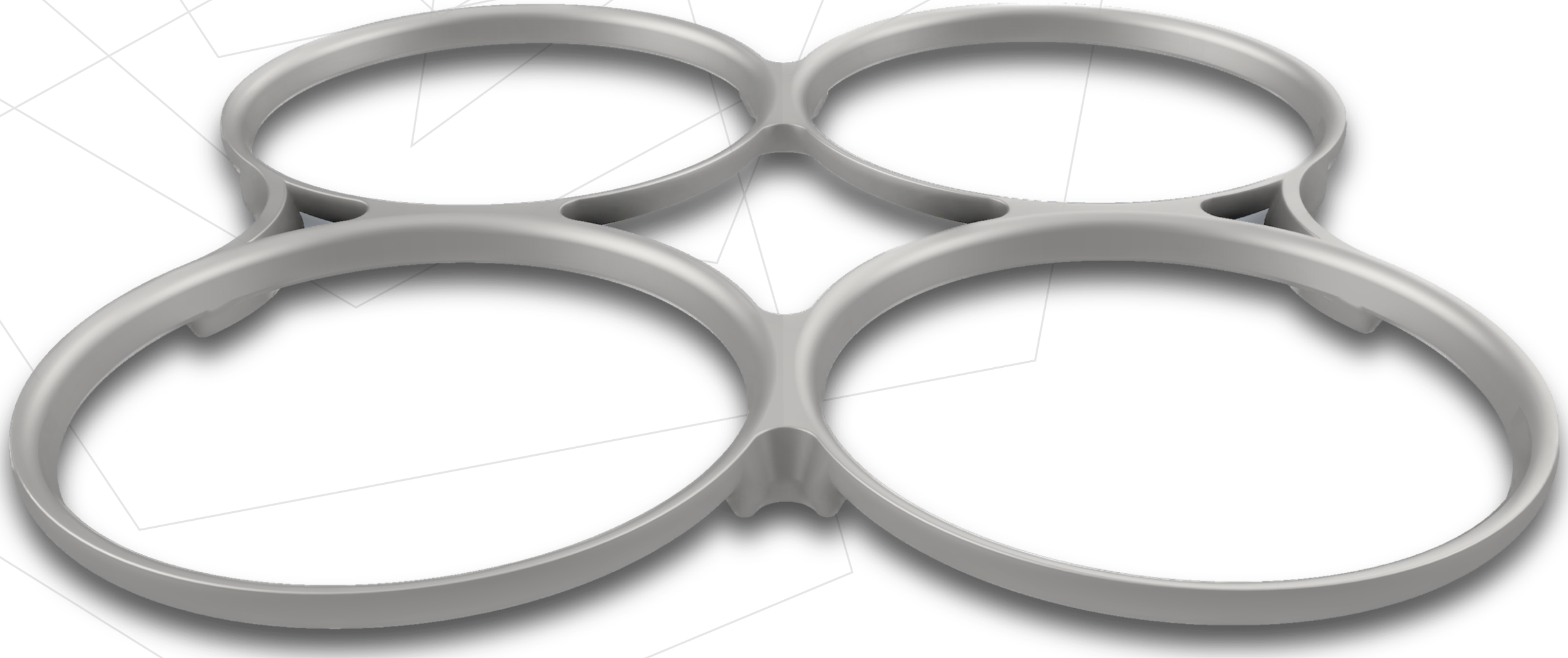

FINITE ELEMENT ANALYSIS OF A 3D PRINTED DRONE/QUADCOPTER BODY

Abraham Martinez Karl Johnson Troy Schmidt

OBJECTIVE

- Model the additive manufacturing processes of a 3D printed drone body using ANSYS
- Analyze the effects of varying AM parameters on the outcome of the part.
  - Deformation
  - Residual Stresses
  - AM Solution Time
  - Temperature Study
- Optimize convergence & simulation time

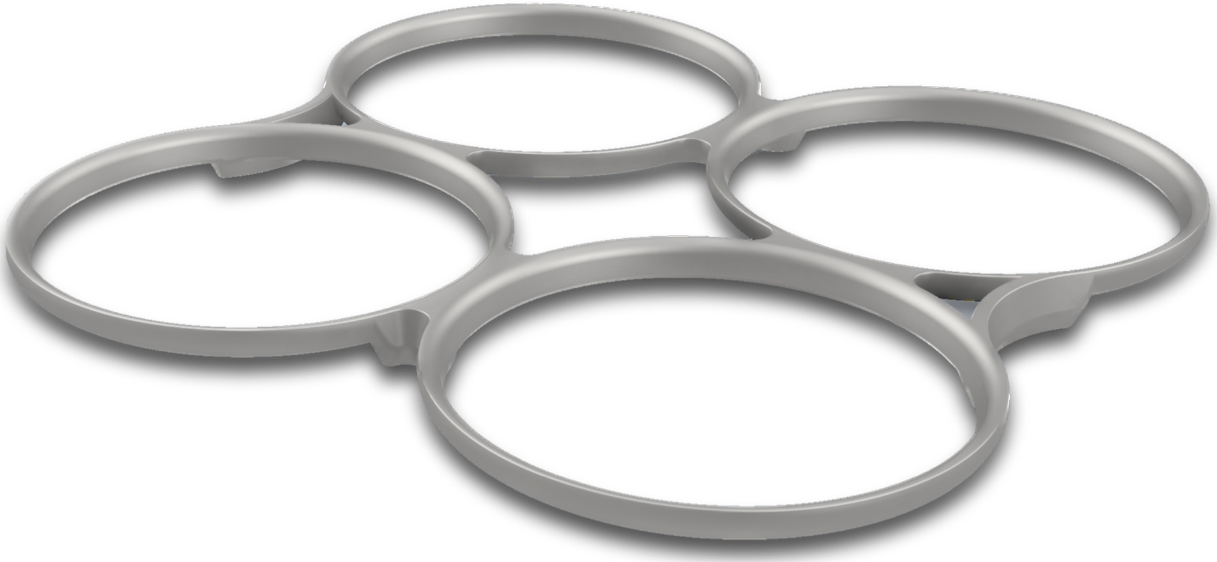

INTRODUCTION- REASONS FOR AM SIMULATION

- Rapid heating and cooling leads to internal stresses
- Internal stress vastly reduces fatigue life
- Internal stress causes dimensional instability

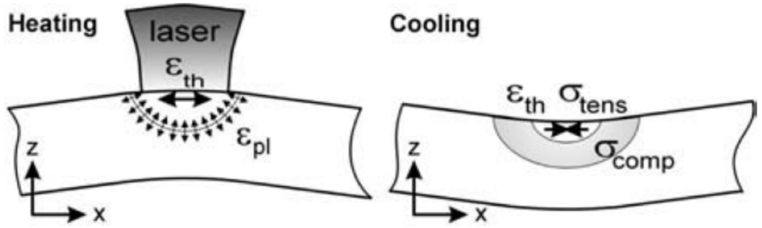

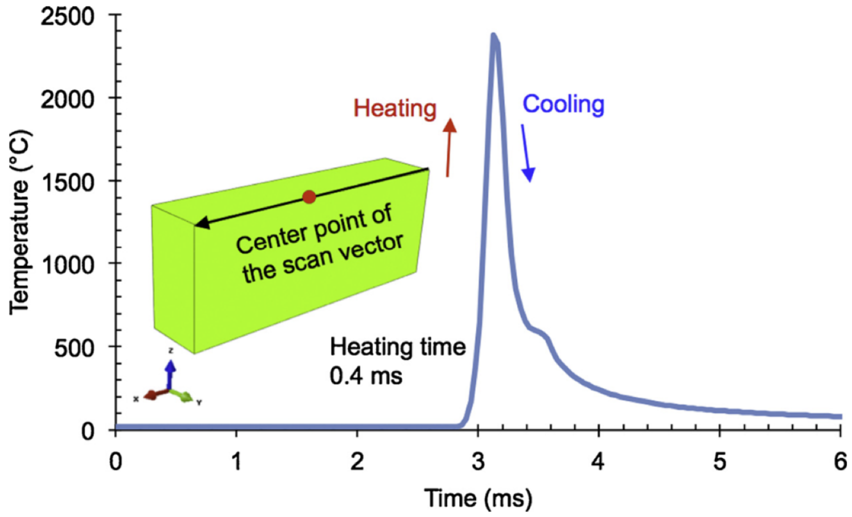

[1]

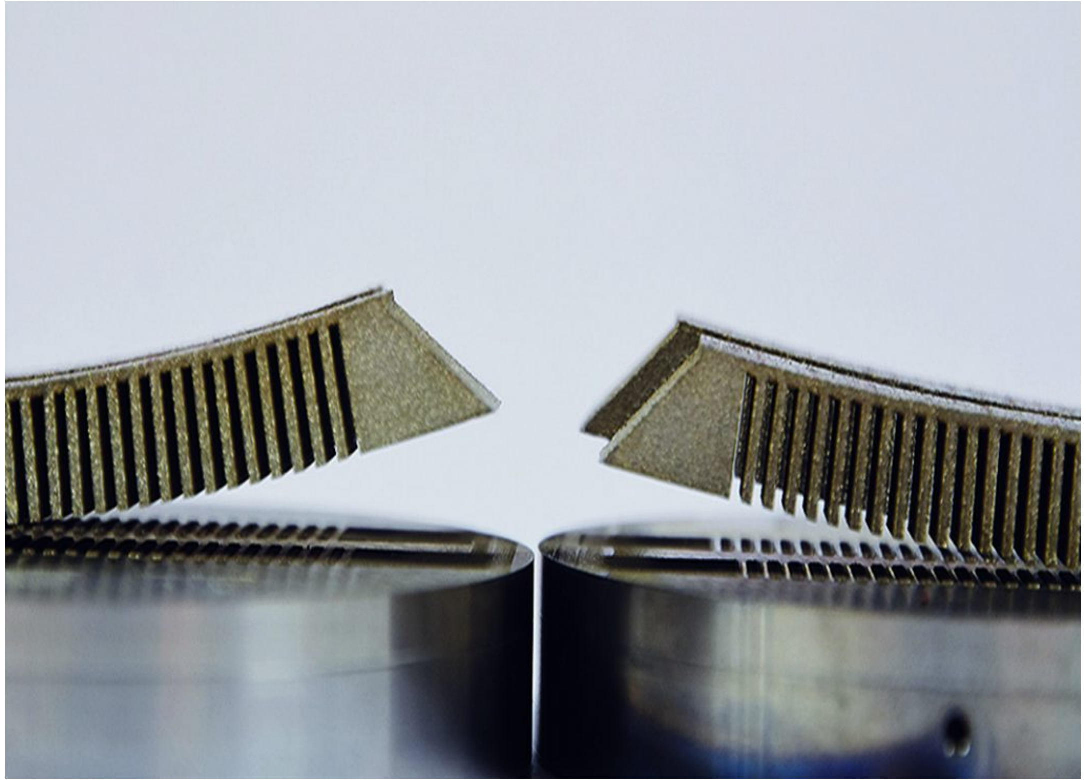

[1]

INTRODUCTION- FUNDAMENTAL EQUATIONS

$$T = \frac{1}{4\pi K R (T - T_0)} \times \left\{ P \exp\left(\frac{-V(R+x)}{2D} \right) - A \left[h(T - T_0) + \varepsilon\sigma (T^4 - T_0^4) + \frac{K(T - T_0)}{R} \right] \right\} + T_0$$

Heat input | Convection | Radiation | Conduction

[3]

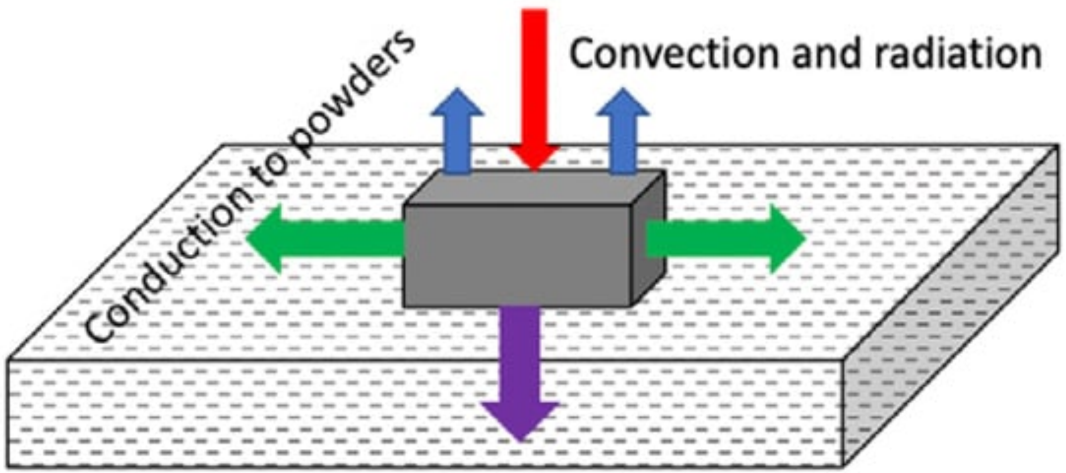

[3]

Coeff. Thermal expansion and elastic modulus | Poisson's ratio | Temperature Gradients

$$\sigma_{xx}(x,z) = -\frac{\alpha(T)E(T)}{1-2\nu(T)} \int_0^{\infty} \int_{-\infty}^{\infty} \left(G_{xh} \frac{\partial T}{\partial x}(x',z') + G_{xv} \frac{\partial T}{\partial z}(x',z') \right) dx'dz' + \frac{2z}{\pi} \int_{-\infty}^{\infty} \frac{p(s)(s-x)^2}{((s-x)^2+z^2)^2} ds - \frac{\alpha(T)E(T)T(x,z)}{1-2\nu(T)}$$

$$\sigma_{zz}(x,z) = -\frac{\alpha(T)E(T)}{1-2\nu(T)} \int_0^{\infty} \int_{-\infty}^{\infty} \left(G_{zh} \frac{\partial T}{\partial x}(x',z') + G_{zv} \frac{\partial T}{\partial z}(x',z') \right) dx'dz' + \frac{2z^3}{\pi} \int_{-\infty}^{\infty} \frac{p(s)}{((s-x)^2+z^2)^2} ds - \frac{\alpha(T)E(T)T(x,z)}{1-2\nu(T)}$$

$$\sigma_{xz}(x,z) = -\frac{\alpha(T)E(T)}{1-2\nu(T)} \int_0^{\infty} \int_{-\infty}^{\infty} \left(G_{xzh} \frac{\partial T}{\partial x}(x',z') + G_{xzv} \frac{\partial T}{\partial z}(x',z') \right) dx'dz' + \frac{2z^2}{\pi} \int_{-\infty}^{\infty} \frac{p(s)(s-x)}{((s-x)^2+z^2)^2} ds$$

$$\sigma_{yy}(x,z) = \nu(T)(\sigma_{xx} + \sigma_{zz}) - \alpha(T)E(T)T(x,z)$$

[3]

INTRODUCTION- AM PARAMETERS

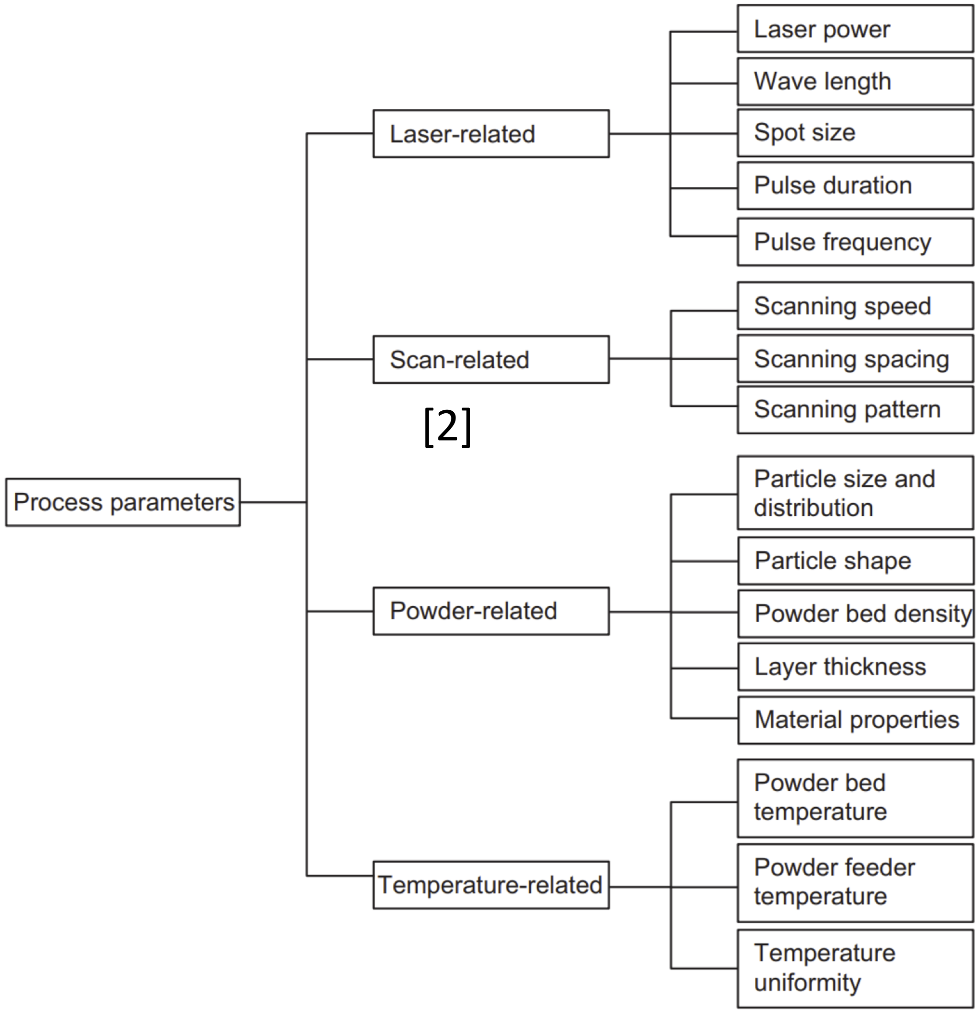

[2]

[2]

- AM parameters shown have varying effects on the melt pool and residual stresses
- Scan speed: Increased speed decrees the linear energy density and lower temp gradient
- Laser power: Increased laser power increases temperature gradient
- Layer Thickness: increased thickness increases porosity and laser power
- Hatch spacing increased hatch spacing decreases build times but also increases porosity
- Not shown: Build Orientation

METHODOLOGY – MESH

- In additive manufacturing on ANSYS, the mesh must be layered
  - Geometries that vary with respect to their height typically require cartesian meshing to accommodate
  - Layered tetrahedron is also regularly used for ANSYS AM processes
  - Tetrahedron mesh will not solve

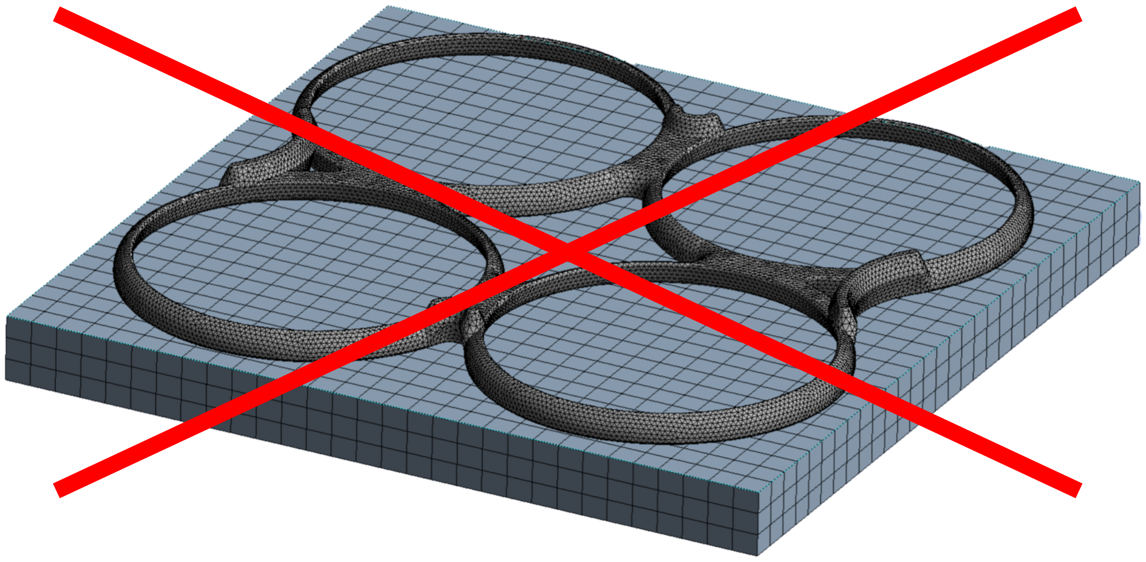

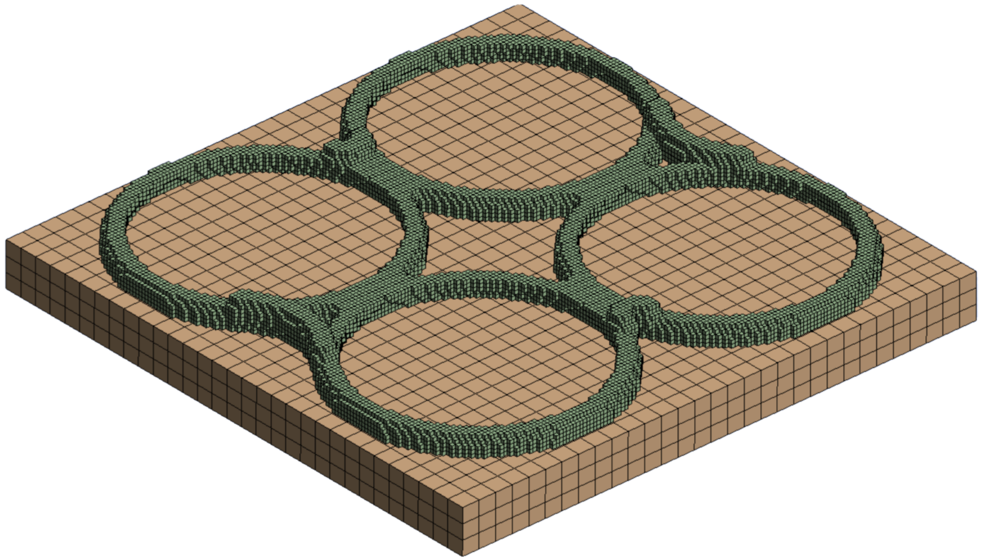

METHODOLOGY – AM PARAMETERS

- 7.5mm mesh size for the first iteration
- 70C temperature at base plate
- Base plate, fixed support
- Baseplate and frame material, 316SS
- Part reference temperature 1370C
- Base reference temperature 50C
- Simplified geometry for first iteration, adding complexity to the model as issues were worked out.

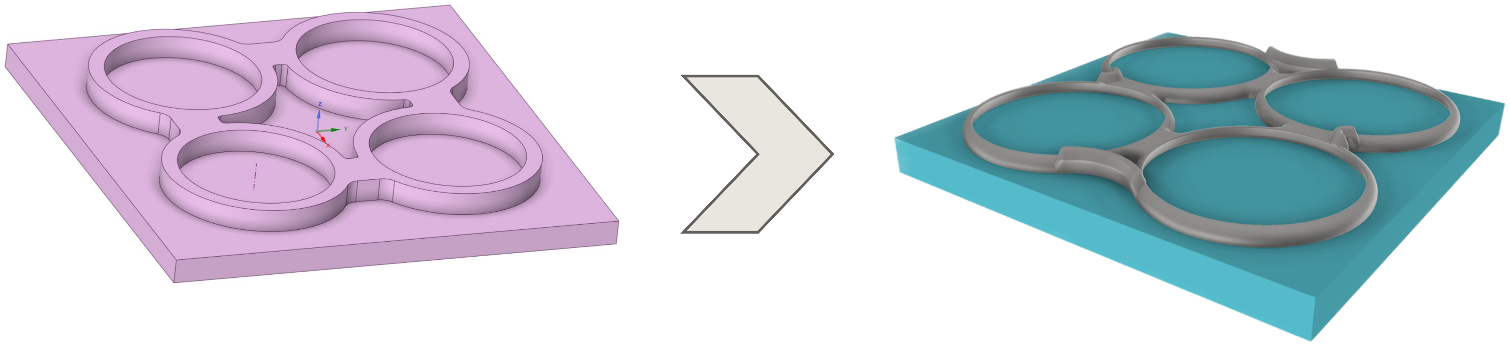

Details of "Build Settings"

Machine Settings	
Additive Process	Powder Bed Fusion
Inherent Strain	No
Thermal Strain Scaling Factor	1.
Deposition Thickness	5.e-002 mm
Hatch Spacing	13. mm
Scan Speed	1200. mm/s
Dwell Time	10. s
Dwell Time Multiple	1.
Number of Heat Sources	1
Build Conditions	
Preheat Temperature	50. °C
Gas/Powder Temperature	Use Preheat Temperature
Gas Convection Coeff	1.e-005 W/mm²·°C
Powder Convection Coeff	1.e-005 W/mm²·°C
Powder Property Factor	1.e-002
Cooldown Conditions	
Room Temperature	22. °C
Gas/Powder Temperature	Use Room Temperature
Gas Convection Coeff	1.e-005 W/mm²·°C
Powder Convection Coeff	1.e-005 W/mm²·°C
Discretization Settings	
Layer Height	Program Controlled

METHODOLOGY – SYMMETRY

- Apply double symmetry and add symmetry boundary conditions

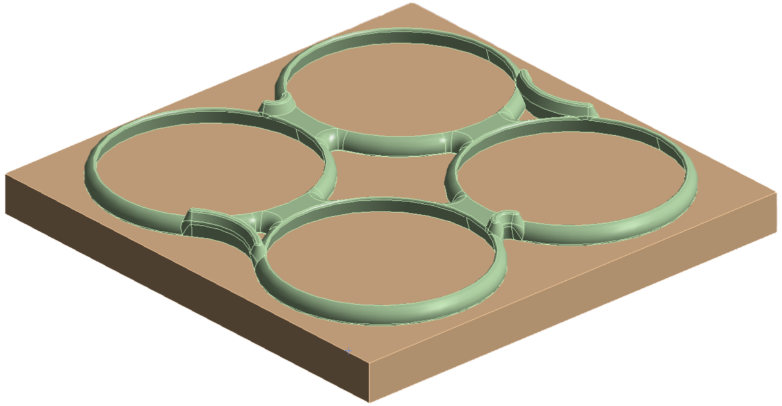

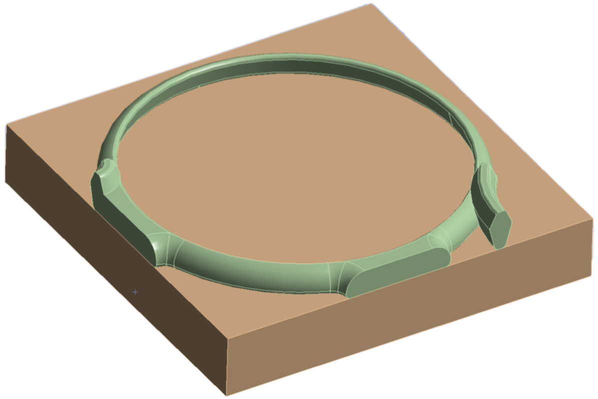

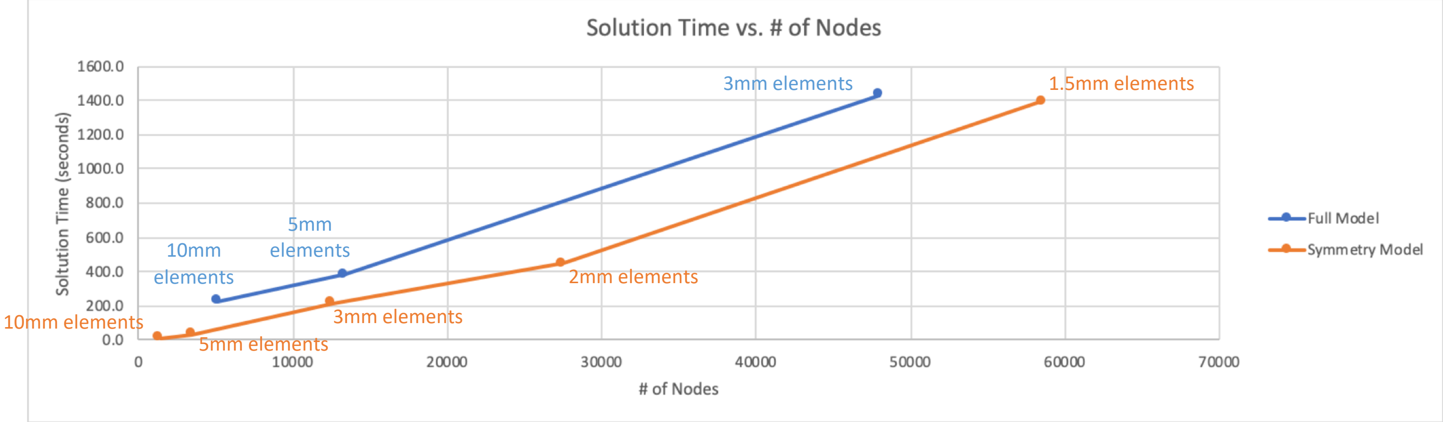

METHODOLOGY – CONVERGENCE

10mm elements

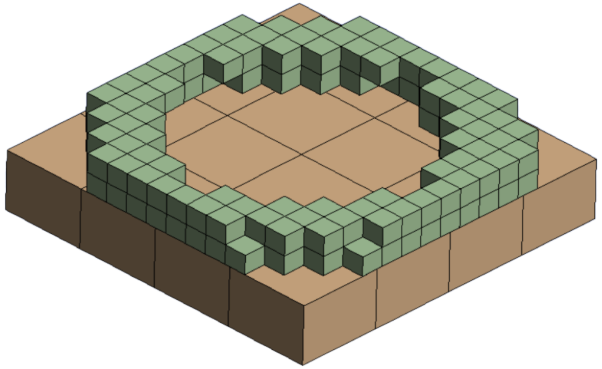

5mm elements

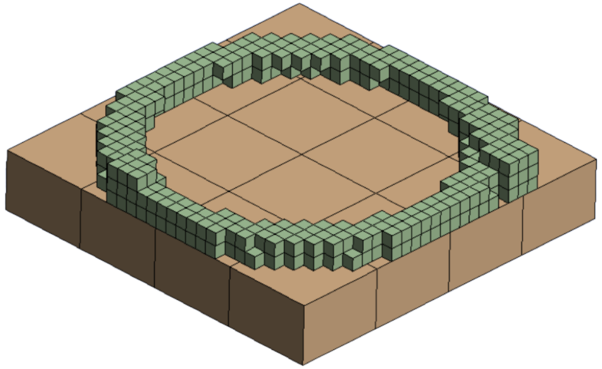

3mm elements

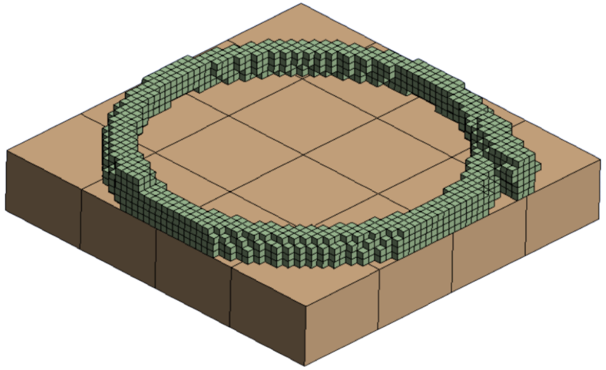

2mm elements

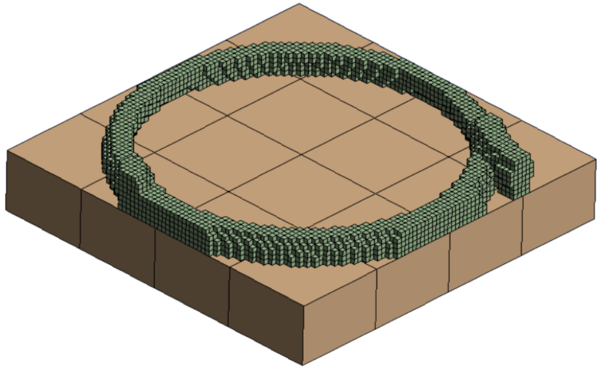

1.5mm elements

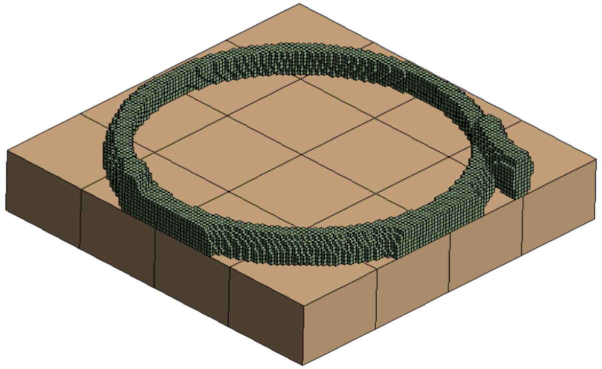

METHODOLOGY – CONVERGENCE

10mm elements

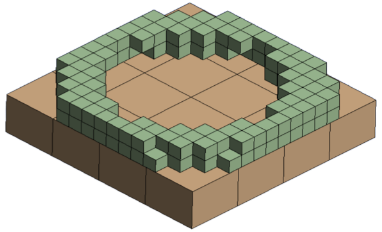

5mm elements

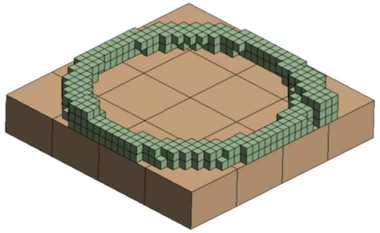

3mm elements

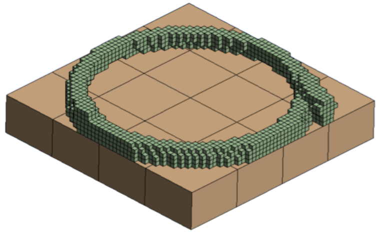

2mm elements

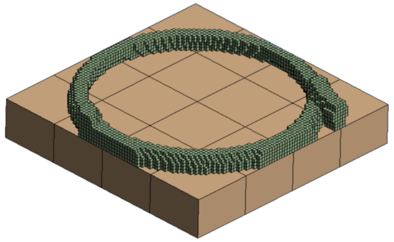

1.5mm elements

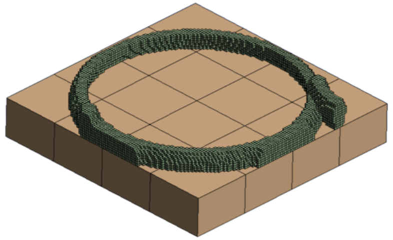

# of Elements	167	465	2041	4844	11052
# of Nodes	1409	3515	12596	27507	58579
Max Deformation	1.082 mm	0.91402 mm	0.75691 mm	0.70786 mm	0.60484 mm
Max Von Mises Stress	417.39 MPa	487.18 MPa	471.71 MPa	492.67 MPa	586.41 MPa
Max Principle Stress	978.07 MPa	1165.9 MPa	1148.9 MPa	1200.6 MPa	2152.9 MPa
Thermal Solution Time	1.4 Seconds	1.9 Seconds	9.5 Seconds	23.0 Seconds	65.5 Seconds
Structural Solution Time	9.2 Seconds	34.3 Seconds	207.5 Seconds	425.1 Seconds	1328.0 Seconds

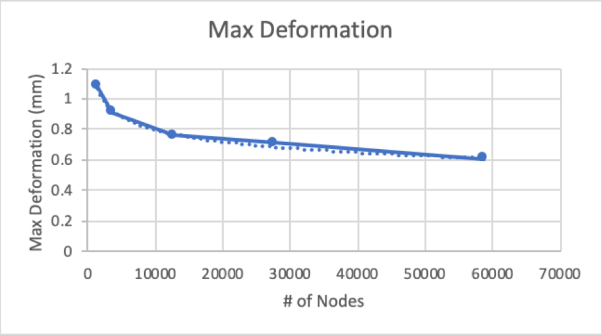

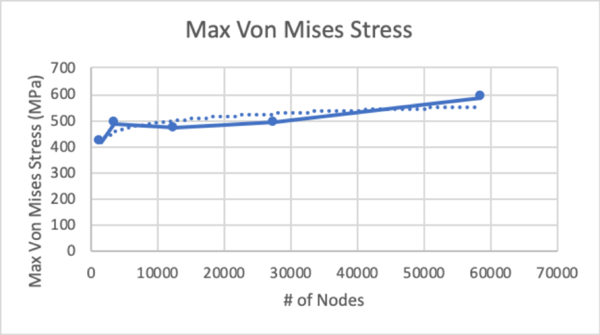

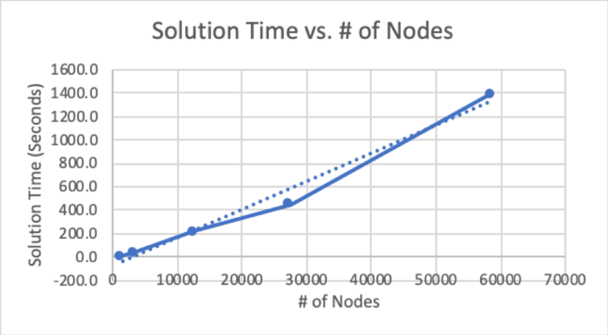

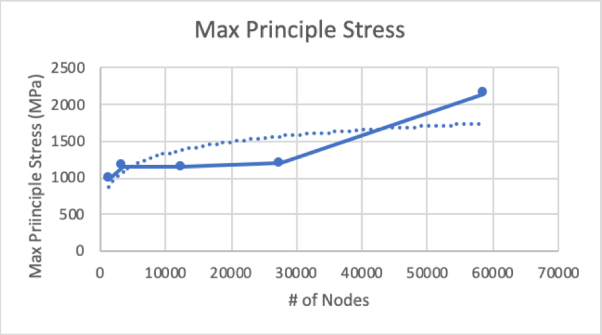

METHODOLOGY – MODIFY GEOMETRY

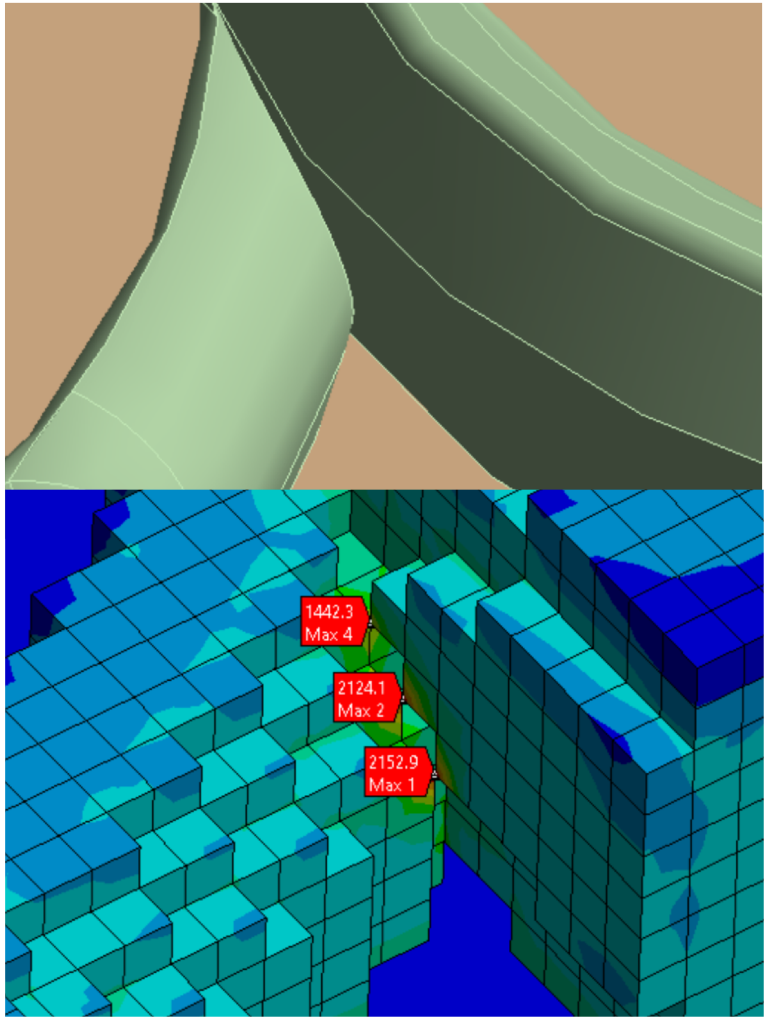

Max Principle Stress @ Sharp Corner: 2152.9 MPa

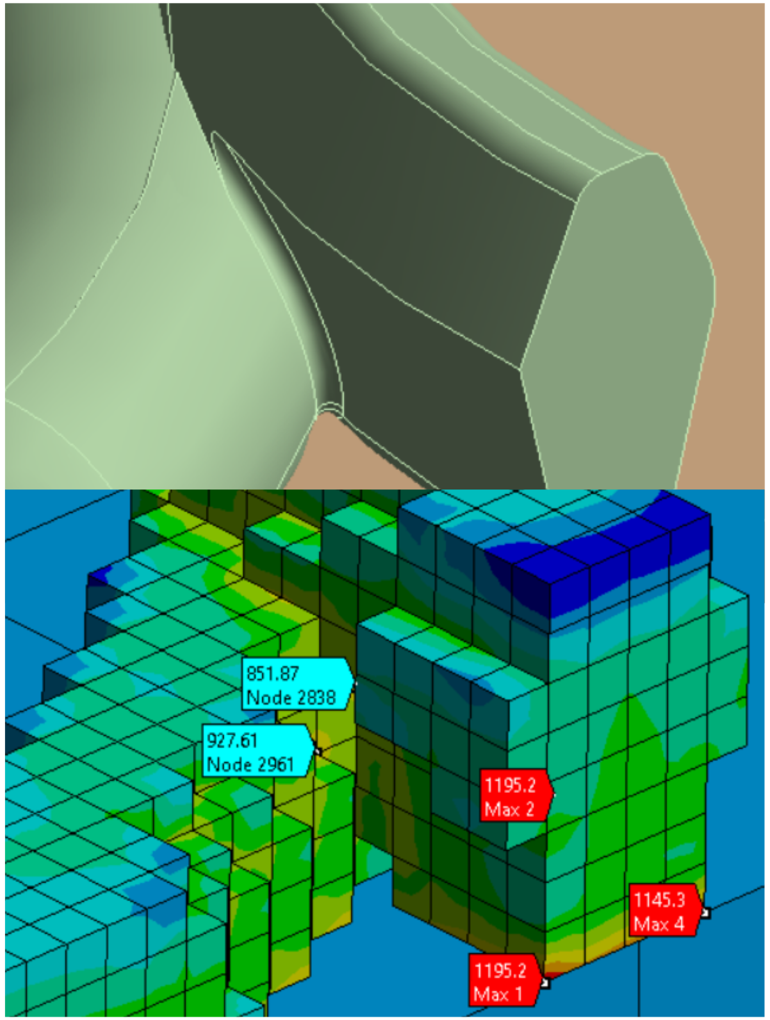

Max Principle Stress @ Fillet: 927.61 MPa

RESULTS – CONVERGENCE OF MODIFIED MODEL

10mm elements

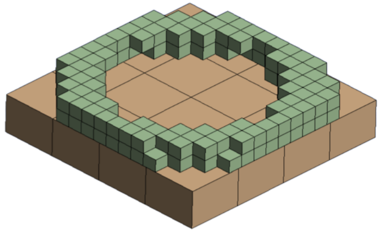

5mm elements

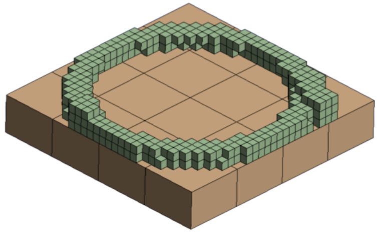

3mm elements

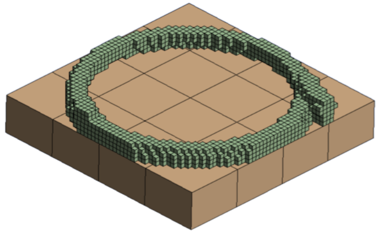

2mm elements

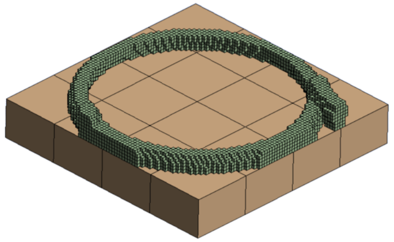

1.5mm elements

Modified Geometry

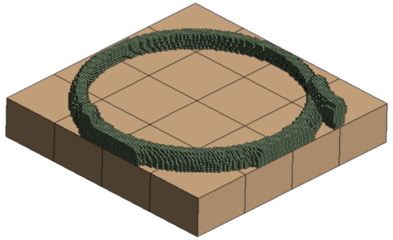

	10mm elements	5mm elements	3mm elements	2mm elements	1.5mm elements Modified Geometry
# of Elements	167	465	2041	4844	11052
# of Nodes	1409	3515	12596	27507	58579
Max Deformation	1.082 mm	0.91402 mm	0.75691 mm	0.70786 mm	0.60484 mm
Max Von Mises Stress	417.39 MPa	487.18 MPa	471.71 MPa	492.67 MPa	487.3 MPa
Max Principle Stress	978.07 MPa	1165.9 MPa	1148.9 MPa	1200.6 MPa	1195.2 MPa
Thermal Solution Time	1.4 Seconds	1.9 Seconds	9.5 Seconds	23.0 Seconds	65.2 Seconds
Structural Solution Time	9.2 Seconds	34.3 Seconds	207.5 Seconds	425.1 Seconds	1326.9 Seconds

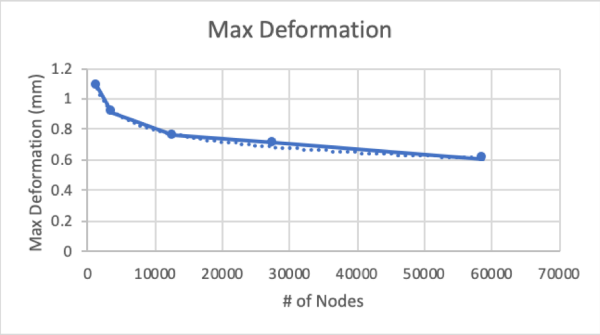

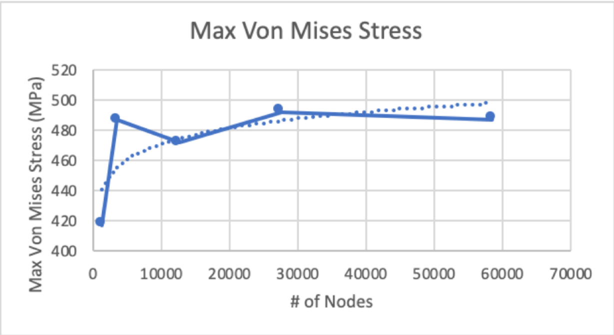

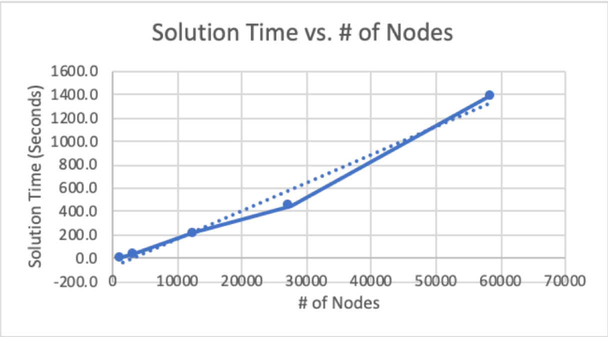

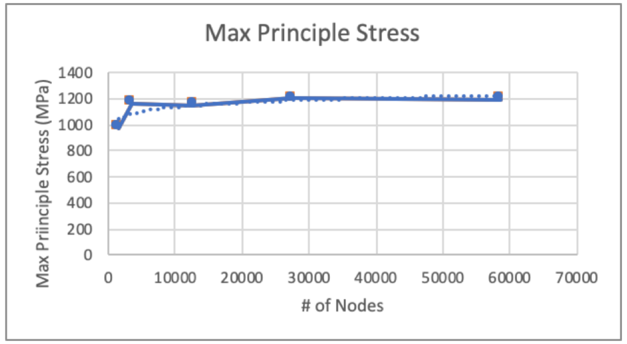

RESULTS – TEMPERATURE STUDY

1.5mm elements

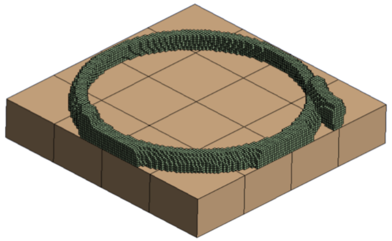

Build Time: 2632.2 S [44 minutes]

Cooldown Time: 3168.7 S [53 minutes]

TOTAL TIME: 1hr 37min

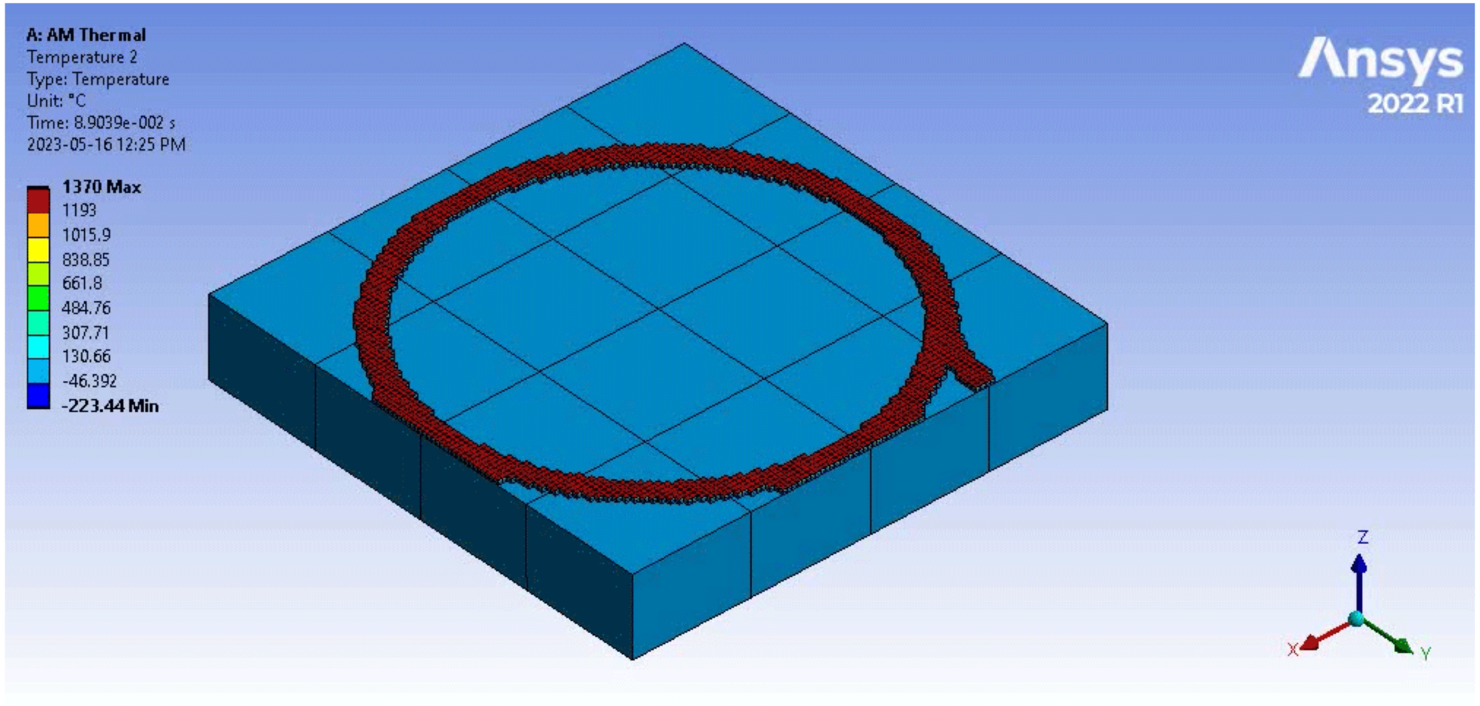

Transient Temperature during Build Step

DISCUSSION/ FUTURE CONSIDERATIONS

Material	Elastic Modulus	Conductivity	Coeff Thermal Expansion	Poissons ratio
Stainless steel	310 GPa	14.4 W/m•K	$16\ \frac{10^{-6}m}{m \cdot C}$	.305
Titanium	120 Gpa	24.5 W/m•K	$9\ \frac{10^{-6}m}{m \cdot C}$	.32
Aluminum	69 GPa	247 W/m•K	$24\ \frac{10^{-6}m}{m \cdot C}$	.334

[7]

- Material
- Build orientation
- Part geometry
- Symmetry
- Node numbering
- Mesh type

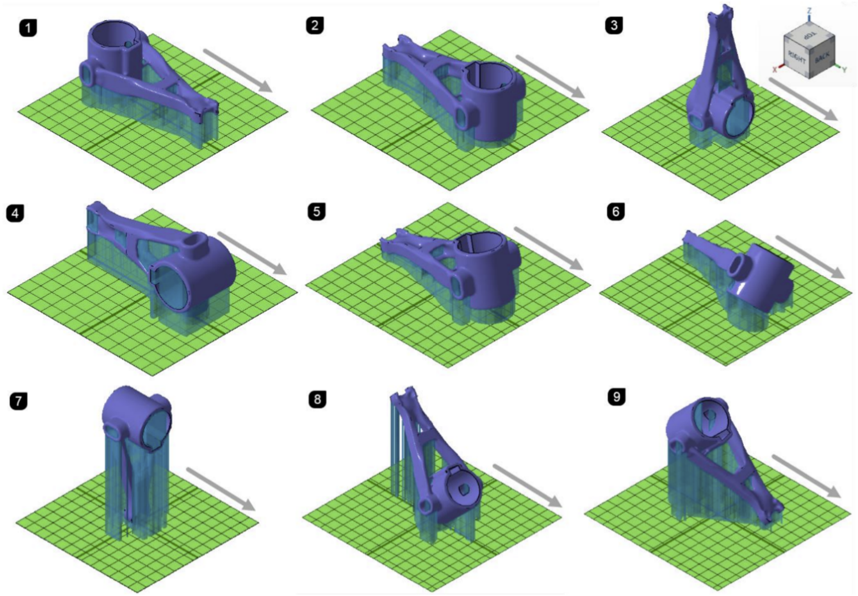

[6]

CONCLUSION

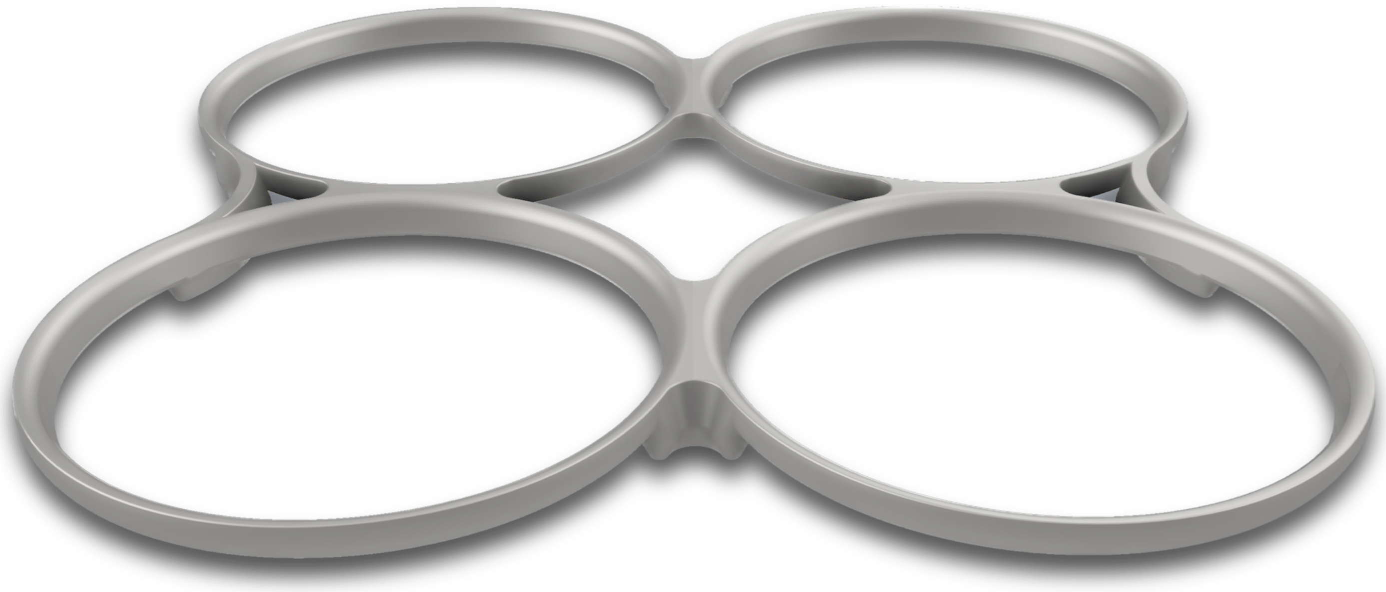

THANK YOU

Abraham Martinez

Karl Johnson

Troy Schmidt

WORKS CITED

[1] C. Li, J. F. Liu, X. Y. Fang, and Y. B. Guo, "Efficient predictive model of part distortion and residual stress in selective laser melting," *Additive Manufacturing*, vol. 17, pp. 157–168, Oct. 2017, doi: https://doi.org/10.1016/j.addma.2017.08.014.

[2] J.-P. Kruth, J. Deckers, E. Yasa, and R. Wauthlé, "Assessing and comparing influencing factors of residual stresses in selective laser melting using a novel analysis method," *Proceedings of the Institution of Mechanical Engineers, Part B: Journal of Engineering Manufacture*, vol. 226, no. 6, pp. 980–991, Mar. 2012, doi: https://doi.org/10.1177/0954405412437085.

[3] S. Sun, M. Brandt, and M. Easton, "Powder bed fusion processes," *Laser Additive Manufacturing*, pp. 55–77, 2017, doi: https://doi.org/10.1016/b978-0-08-100433-3.00002-6.

[4] E. Mirkoohi, H.-C. Tran, Y.-L. Lo, Y.-C. Chang, H.-Y. Lin, and S. Y. Liang, "Analytical Modeling of Residual Stress in Laser Powder Bed Fusion Considering Part's Boundary Condition," *Crystals*, vol. 10, no. 4, p. 337, Apr. 2020, doi: https://doi.org/10.3390/cryst10040337.

[5] H. Hyer and C. M. Petrie, "Effect of powder layer thickness on the microstructural development of additively manufactured SS316," vol. 76, pp. 666–674, Apr. 2022, doi: https://doi.org/10.1016/j.jmapro.2022.02.047.

[6] R. Magana-Carranza, C. J. Sutcliffe, and E. A. Patterson, "The effect of processing parameters and material properties on residual forces induced in Laser Powder Bed Fusion (L-PBF) ," 2021.

[7] M. Pagac *et al.*, "Prediction of Model Distortion by FEM in 3D Printing via the Selective Laser Melting of Stainless Steel AISI 316L," *Applied Sciences*, vol. 11, no. 4, p. 1656, Feb. 2021, doi: https://doi.org/10.3390/app11041656.

[8] "Poisson's ratio," *Engineeringtoolbox.com*, 2019. https://www.engineeringtoolbox.com/poissons-ratio-d_1224.html

[9] *Ansys® Workbench, Release 22.2*

[10] Autodesk Inventor, 2022